Journal of Theoretical and Computational Chemistry
Vol. 13, No. 7 (2014) 1450055 (18 pages)

DOI: 10.1142/S0219633614500552

DFT study on the interaction between atomic aluminum and graphene

Nicolás F. Domancich*, Ricardo M. Ferullo† and Norberto J. Castellani*,‡

*Grupo de Materiales y Sistemas Catalíticos, Instituto de Física Sur
Departamento de Física, Universidad Nacional del Sur
Avenida Alem 1253, 8000 Bahía Blanca, Argentina

†Instituto de Química del Sur
Departamento de Química, Universidad Nacional del Sur
Avenida Alem 1253, 8000 Bahía Blanca, Argentina
‡castella@criba.edu.ar

Received 29 April 2014
Accepted 4 September 2014
Published 20 October 2014

In the present work, molecular orbital calculations using cluster models were performed within density functional theory (DFT) in order to study the adsorption of an Al atom on regular and defective graphene. Depending on the theoretical treatment of electronic exchange and correlations effects, different bonding results for the adsorption on the perfect surface are obtained. On the other hand, they are very similar for Al adsorbed on a carbon monovacancy. On regular graphene, the adsorption is exothermic when the Perdew, Burke and Ernzerhof (PBE) functional is used and endothermic with the Becke, 3-parameter, Lee–Yang–Parr (B3LYP) functional. Regarding the defective graphene surface, it was shown that the carbon atoms of concave angles in the vacancy are the most reactive to a radical attack. The adsorption of an Al atom on the vacancy restores the trigonal symmetry lost after the extraction of the C atom from regular graphene. Complementary calculations performed at PBE level on both regular and defective surfaces imposing periodic conditions qualitatively support the results obtained with the cluster model.

Keywords: Graphene; monovacancy; aluminum; adsorption; DFT.

1. Introduction

In the last two decades, a significant part of nanoscience and nanotechnology advances have been related to the development of carbon nanostructures where carbon atoms have sp^2 hybridization. More recently, research on the parent structure represented by graphene has received huge impulse due to the interest in knowing the rules governing its impressive electronic and mechanical properties in conjunction with its rich chemical behavior. It is highly interesting to widen graphene

‡Corresponding author.

applicability modifying its intrinsic properties by coupling this material with other species such as atoms, molecules and nanoclusters that exhibit attractive physicochemical properties at the nanoscale. Particularly, the adsorption of individual atoms on the graphene honeycomb lattice is relevant because new electronic states are added near the Fermi level changing its response to external electric fields. Theoretical examination of different atom/graphene systems is of interest in the development of new electronic devices and in the production of bidimensional magnetic structures with magnetism localized on the adsorption sites.[1,2]

The study of the interaction of a nontransition metal atom with graphene is relevant from a fundamental point of view because only s–p orbitals of adsorbate are implied. An earlier work performed by Chan *et al.*,[3] in the framework of density functional theory (DFT) and with the Perdew, Burke and Ernzerhof (PBE) functional for different metallic atoms adsorbed on perfect graphene showed that an intermediate — neither strong nor definitively weak — interaction of chemisorptive nature has been produced. This interaction is accompanied by a relevant drift of electronic charge from the adsorbed to the substrate atoms, which is compatible with the existence of metal-carbon ionic bonds. In the case of the alkaline metals, magnetization of the adsorbed atom decreases noticeably in comparison with the isolated species. For the alkaline earth metals, instead, it changes from zero to a value near $1\,\mu_B$.

The interest to study the adsorption of alkaline metals on graphene is particularly relevant because the alkaline metal/graphene systems constitute proposals of combined materials for hydrogen storage. The calculations for Li/graphene based on PBE[3] or Lee–Yang–Parr (B3LYP)[4] functionals point out the presence of a chemisorptive interaction where the Li–C bonds are shorter than the sum of their covalent radii, with an electron transfer from the metal to the graphene. From a thermodynamic point of view, in these two approaches for the exchange and correlation functional the interaction is exothermic. On the other hand, calculations performed within the second-order Møller–Plesset (MP2) formalism[5] support the existence of exothermic states of physisorption nature at adsorbate-substrate distances of about 3 Å while at shorter distances of about 2 Å only endothermic states are produced. More recently, DFT results based on the PBE functional sustain the presence of exothermic states at relatively short Li-graphene distances.[6]

Recent calculations for Be atom adsorbed on graphene at PBE level with semiempirical corrections for dispersive forces[7] show the presence of exothermic physisorption states at Be-graphene distances of about 3 Å, while for shorter distances endothermic states are also predicted, similarly as the results for the Li/graphene system.[5]

Regarding the adsorption of individual atoms of aluminum, an element of group III, previous DFT calculations[3] using the PBE functional show similar behavior to that of alkaline and alkaline-earth metals, although it is noteworthy that earlier results obtained with the Hartree–Fock (HF) method do not report the formation of stable chemisorption bonding for the Al/graphene system.[8] It is an open question

whether this metal follows the same trends that alkaline and alkaline-earth metals and in what measure its predicted adsorption properties on graphene depends on the exchange and correlation functional used in DFT calculations.

The doping of graphene with heteroatoms of III and V groups has been used as a way to get a nonzero band gap, allowing the use of modified graphene as gate material in field effect transistors (FET).[9] Besides, the presence of these defects induces electron spin polarization locally, highly relevant in systems predominantly with s–p bands. The combination of these transport and magnetic properties of electrons is very attractive in the domain of spintronics.[2] On the other hand, it has been proposed that, considering its chemical affinity against certain molecules, the incorporation of a particular heteroatom to the graphene lattice would make it a very specific sensor for gases, for example, by testing the ohmic response of doped graphene as well as measuring the characteristic current–voltage curves of a FET with this material in the gate.[10,11] In the specific case of an Al heteroatom, several theoretical works have been reported concerning to the adsorption of diatomic (CO, NO, O_2, H_2),[12–15] triatomic (NO_2, SO_2, CO_2, H_2O)[13,14] and larger molecules (NH_3, H_2CO).[13,14,16] It should be underlined that in all the inherent calculations with Al and other heteroatoms, only the PBE functional for exchange and correlation was employed.

In the present work, the adsorption of individual atoms of aluminum on perfect graphene and on defective graphene with carbon monovacancies was considered. To that purpose, molecular orbital calculations were performed using the cluster model with a local basis in the context of DFT formalism. In this way, a fairly transparent view of Al–C bonds regarding particularly the role played by electron spin localization and charge transfer was obtained. The results calculated with the PBE functional for exchange and correlation were compared with those corresponding to the B3LYP functional. These results were further compared with those obtained from a periodic model using a plane-wave basis set.

2. Computational Details

The present calculations are based on DFT and were carried out mainly applying a cluster model with a localized Gaussian basis set. This approach was accomplished appealing to the Gaussian-03 package.[17] To study the adsorption of one Al atom on a regular graphene sheet, a surface model consisting with a central hexagonal C_6 unit surrounded by two consecutive crowns of C_6 units and saturated with H atoms was implemented. The resulting structure was that of the circumcoronene molecule ($C_{54}H_{18}$). In the case of Al adsorption on a carbon vacancy of graphene, four central C_6 units surrounded by one crown of C_6 units also saturated with H atoms was used. The resulting structure can be ascribed to that of the circumpyrene molecule without its central C atom ($C_{41}H_{16}$). Clusters of similar size have been used in the past to represent the surface of graphene.[18–24] Calculations for the cluster model were performed applying the PBE exchange and correlation functional due to PBE[25] and the

B3LYP hybrid functional,[26] both at the unrestricted spin level. E_{ads} was computed according to:

$$E_{ads} = E_{Al/substrate} - E_{Al} - E_{substrate}, \quad (1)$$

where $E_{Al/substrate}$, E_{Al} and $E_{substrate}$ correspond to the Al/substrate, isolated Al atom and substrate total energies, respectively. In this way, a negative E_{ads} means an exothermic process. Adsorption energy values have been corrected by the basis set superposition error (BSSE) using the counter-poise (CP) correction.[27] The Al-graphene distance taken from the graphene sheet and the coordinates corresponding to the nearest C atoms to Al were optimized looking for the E_{ads} minimum. In all the calculations the 6–31++G** basis set was used. Atomic net charges (Q) and spin population (SP) were calculated by means of the natural population analysis (NPA).[28]

Complementary calculations were performed considering a slab model. This approach to the Al/graphene system was accomplished appealing to the Vienna *ab-initio* simulation package (VASP).[29,30] It solves the Kohn–Sham equation of DFT using a plane wave basis set. A good convergence was achieved with cut-off energy of 700 eV for the kinetic energy. The projector augmented wave (PAW) method was used to describe the effect of the core electrons on the valence states.[31,32] The exchange and correlation effects were calculated by the PBE functional. The two-dimensional Brillouin integrations were performed on a grid of $5 \times 5 \times 1$ Monkhorst–Pack special k-points.[33] All the calculations were performed at the spin-polarized level. Graphene was represented by means of a 4×4 supercell with 32 carbon atoms and a gap of 20 Å in the normal direction to the sheet of graphene. This vacuum gap is large enough to avoid interaction between the adsorbed Al atoms and the periodic images of the slab. All the atoms within the supercell were allowed to relax until the residual Hellmann–Feynman forces were low than 0.01 eV/Å. A large box of $20 \times 20 \times 20$ Å^3 was used to obtain the gas-phase atomic Al energy.

3. Results and Discussion

3.1. *Al adsorption on regular graphene*

The adsorption of one Al atom was considered on the three highly symmetric sites of a graphene sheet: top, bridge and hollow. In Fig. 1, the corresponding sites for the cluster model are schematized. The slab model was also schematized in the same figure for the hollow site. Table 1 summarizes E_{ads} values and the equilibrium geometric data; i.e., Al–C distance and Al and C deviations from the perfect planar surface.

From Table 1 we observe that at PBE level adsorption energies correspond to an exothermic process; i.e., the local minimum of total energy for Al/graphene system near the graphene surface is lower than the total energy for isolated Al and the substrate. The values of adsorption energies correspond to weak chemisorption

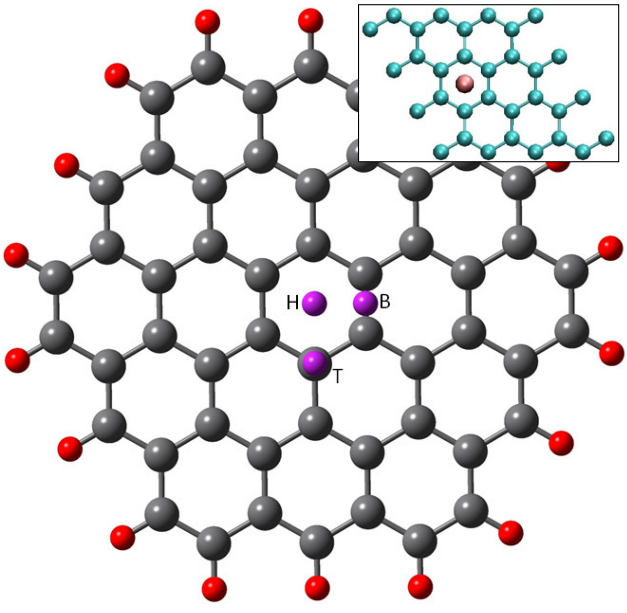

Fig. 1. (Color online) Cluster model for the adsorption geometries of Al adsorbed on regular graphene. T: on Top, B: Bridge and H: Hollow. C atoms: large grey balls; Al atom: small light blue ball; H atoms: small red balls.The inset shows the geometry for the hollow site on the slab model.

states. The hollow and bridge sites are the most favored, with the site favoring: hollow > bridge > top. E_{ads} values difference between the highest and lowest sites, which could be assimilated to the minimal activation energy for migration on the graphene surface, is of 0.08 eV. The Al–C distances (2.3 Å–2.6 Å) obtained with the cluster model are 0.1 Å–0.4 Å larger than the sum of Al and C covalent radii,

Table 1. E_{ads} and geometrical parameters for Al adsorption on regular graphene. h_{Al} (h_C) is the distance between Al (C) and the perfect planar graphene.

		E_{ads}(eV)[a] Top/Bridge/ Hollow	d_{Al-C}(Å)[b] Top/Bridge/ Hollow	h_{Al}(Å) Top/Bridge/ Hollow	h_C(Å)[b] Top/Bridge/ Hollow
Cluster model	PBE	−0.28/ − 0.36/ − 0.36	2.29/2.39/2.57	2.29/2.29/2.14	−0.01/0.02/ − 0.01
	B3LYP	NB/0.10/0.13	NB/2.44/2.62	NB/2.36/2.19	NB/0.03/0.00
Slab model	PBE	−0.84/−0.86/−0.96	2.26/2.40/2.55	2.20/2.20/2.11	−0.05/ − 0.02/0.00
	PBE[c]	−0.91/ − 0.93/ − 1.04	2.24/2.33/2.56	2.22/2.22/2.13	−0.02/ ± 0.01/ ± 0.01
	LDA[d]	−0.88/ − 0.90/ − 0.79	2.40/2.47/2.65	2.40/2.35/2.23	—

[a]NB: Nonbonding.
[b]C: First nearest neighbor from Al atom.
[c]Work of Chan *et al.*,[3]
[d]Work of Moullet.[33]

*c.*2.20 Å, and the Al–C distance in trimethylaluminum (1.97 Å–2.14 Å),[34] suggesting the formation of a relatively weak chemical bond between adsorbate and substrate.

Looking at the results of Table 1 obtained with the slab model, we observe that they are appreciably larger in magnitude than those of the cluster model by about 0.6 eV. The hollow site is the most favored, followed very nearly by the bridge site. The migration energy is quite similar, 0.12 eV, and the Al–C distances are very near to those obtained with the cluster model, varying by +0.03, −0.01 and +0.02 Å for top, bridge and hollow sites, respectively. Earlier calculations performed using the same theoretical approach as that used here reached adsorption energy values *c.* 0.07 eV larger in magnitude and Al–C distances very near than our results; namely, 0.05, 0.06 and 0.01 Å longer for top, bridge and hollow sites, respectively.[3] Therefore, different approaches performed with the PBE functional favor the hollow site consistently. Looking at the values of the C deviations from the perfect planar surface in Table 1, we observe that a small or negligible puckering of the graphene surface is obtained both in the cluster and slab models. Particularly, the most favored hollow site shows minimal puckering.

Besides, in the case of previous calculations performed using periodic conditions and a plane wave basis set,[35] but with the local density approximation (LDA) functional, the top site becomes the most favored site — with the bridge site very near in stability — presenting E_{ads} values slightly lower in magnitude, 0.03 eV, than those obtained with the PBE functional. The corresponding Al–C distances are 0.06 Å–0.14 Å larger. In another series of LDA calculations for different types of atoms adsorbed on graphene, it was shown that for Al/graphene the top site is favored with a relatively large magnitude for the E_{ads} value, −1.6 eV, and at a short Al–C distance, 2.04 Å.[36]

Considering again the results for the cluster model in Table 1, but focusing now on those corresponding to the B3LYP functional, we notice that in contrast with the PBE functional the adsorption energies obtained with the B3LYP functional correspond to an endothermic process for the bridge and hollow sites, whereas no minimum is present for the on-top geometry. E_{ads} values are 0.45 eV–0.50 eV higher than those obtained with the PBE functional, favoring the bridge site–the hollow site is only 0.03 eV less stable. The Al–C distances are concomitantly 0.04 Å–0.08 Å larger than those calculated with PBE. Contrary to PBE, surface puckering is larger for the most favored site. No other reported values have been published in the literature using this hybrid functional and concerning the Al/graphene system.

Very recently, DFT calculations performed with PBE have also predicted the existence of metastable states for Be atom adsorbed at nearly 1.8 Å from the graphene surface[7] and with an adsorption energy of about 0.5 eV, i.e., an endothermic state from the thermodynamic point of view. On the other hand, a similar behavior at short adsorbate-substrate distance was obtained by means of the MP2 formalism for the Li/graphene system,[5] where a metastable state was observed at about 1.8 Å with an energy of near 1.6 eV above the free atom limit, revealing an important repulsive component, as predicted by HF calculations.[5]

As it will be shown later, the bonds established for Al adsorbed on the hollow and bridge sites and described with the B3LYP functional imply an important electron transfer, similarly as the results obtained with PBE. Hence, the attractive contribution of ionic nature to E_{ads} should be counterbalanced by a significant repulsion probably due to the different treatment given by B3LYP to the electronic exchange and correlation effects. Taking into account the results obtained using MP2 and HF for Li/graphene,[5] it can be concluded that the exact exchange component of B3LYP functional could be the main responsible for that repulsive behavior. Interestingly, earlier results obtained at the HF level and using a cluster of similar size ($C_{52}H_{18}$) with the notion of the so-called "prepared states" for adsorption, have shown that an Al atom does not adsorb at short distances — less than 3 Å — on graphene.[8]

In Table 2, the charges calculated with the NPA method for Al and its nearest neighbors in the graphene surface are summarized. Notice that an important electronic charge transfer occurs from Al to the graphene surface, the Al atom attaining 0.7 e–0.8 e with both PBE and B3LYP functionals. This charge polarization of Al–C bonds has been evidenced in previous DFT calculations, regarding the spatial electronic charge distribution and the formed dipole moment.[3]

In the calculations performed with the cluster model both the doublet and quadruplet were considered as possible electronic states. The quadruplet state was always higher in energy than the doublet; hence, any magnetism is due to one unpaired electron. In Table 2, the atomic SP values calculated from the α- and β-spin NPA populations are also summarized. Notice that on the Al and its C neighboring atoms resides 0.22 (PBE) and 0.28 (B3LYP), or less, of the SP corresponding to the doublet configuration, indicating that the spin becomes largely delocalized. This last observation is in line with the results obtained with our slab model where the nonmagnetic system becomes more favored energetically and also with those of other reported periodic approaches.

We also have observed that neither PBE nor B3LYP predict Al physisorption at large distances (about 3 Å) such as found for Li adsorption using MP2.[5] This result is not surprising because it is well-known that DFT fails in describing van der Waals interactions. We have performed complementary high-level calculations using the Al/circumcoronene model at MP2/6-31G** level (adsorbed on hollow site). Two

Table 2. NPA atomic net charge (Q) and atomic spin population (SP) for Al adsorption on regular graphene (Cluster Model).

	Q[a] Top/Bridge/Hollow	SP[a] Top/Bridge/Hollow
PBE	Al: 0.72/0.71/0.82	Al: 0.14/0.16/−0.01
	C: −0.23/−0.20/−0.10	C: 0.04/0.06/0.03
B3LYP	Al: —/0.68/0.83	Al: —/0.21/−0.01
	C: —/−0.19/−0.09	C: —/0.07/0.04

[a]C: First nearest neighbor from Al atom.

minima were observed, at about 2.1 Å and 3.2 Å, with adsorption energies of −0.45 eV and −0.25 eV, respectively. Thus, the result obtained at short distance is similar than the one calculated with PBE and the cluster model. However, the strength bond between Al and graphene seems to be overestimated with PBE and the slab approach. The detailed calculations carried out with MP2 will be published in a separated work, where the effect of van der Waals interactions on DFT calculations is also considered.

The results of this section suggest that studying the interaction between an Al atom and a pristine graphene sheet is difficult to address. Indeed, we observed that while with the PBE functional the ionic interaction due to Al to C charge transfer predominates and an exothermic adsorption is obtained, with the B3LYP functional an important repulsion overcomes the ionic interaction and an endothermic adsorption is produced.

3.2. *The carbon monovacancy*

Usually the main objective of theoretical approaches to graphene doped with a heteroatom such as Al is to describe its electronic structure in terms of band concepts which include the local density of states, the opening of the band gap or the formation of new localized states. On the other hand, it is very important to conceive this system as the result of the adsorption of an Al atom on a previously formed monovacancy in graphene. For that reason, we firstly describe the relevant chemical aspects of defective graphene.

The creation of a carbon vacancy has been analyzed according to the following mechanism:

$$\text{Graphene} \rightarrow \text{Graphene (vacancy)} + \text{isolated C atom}, \tag{2}$$

whose energy balance is defined as the monovacancy formation energy, E_{vac}, which can be calculated considering two contributions:

$$E_{\text{vac}} = E_{\text{extrac}} + E_{\text{relax}}. \tag{3}$$

E_{extrac} corresponds to the extraction of a C atom giving a nonrelaxed defective structure and E_{relax} to the geometrical relaxation of this last step. In Fig. 2, the corresponding geometries for the cluster model before and after the creation of the vacancy are schematized. In Table 3, the values for E_{vac} and E_{relax} and the main geometrical parameters are summarized.

Observing the results of our cluster model in Table 3, we notice that both PBE and B3LYP give similar values for the E_{vac} energy, *c.* 15.5 eV. The PBE result is only 0.2 eV larger than the B3LYP one. Noticeably, while the E_{relax} term contributes only a little to E_{vac}, *c.* 3%, the optimized structure obtained for the vacancy shows a visible distortion. The vacancy geometry corresponds to a polygon with 12 sides, 3 concave C–C–C angles with their vertex pointing toward the defect center and 9 convex C–C–C angles with their vertex pointing outside the defect. The geometrical parameters obtained with our cluster model are very similar for both functionals and

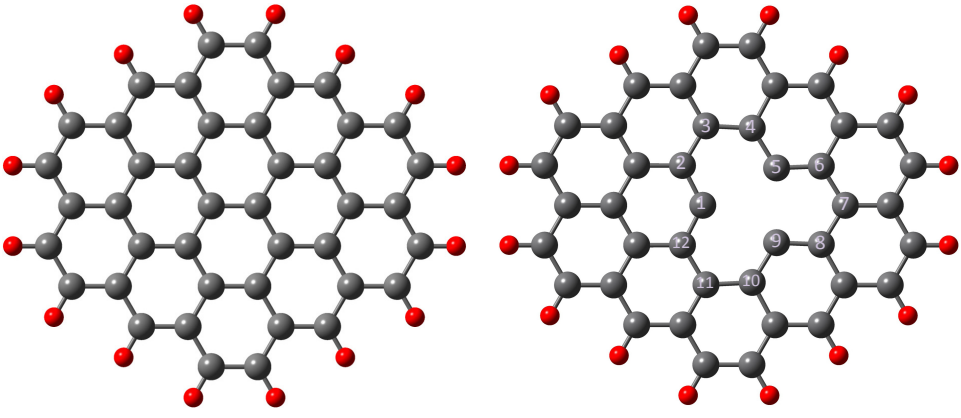

(a) (b)

Fig. 2. (Color online) Cluster model for a carbon vacancy creation in graphene. C atoms: large grey balls; H atoms: small red balls. Top panel: regular graphene. Bottom panel: graphene with a monovacancy. Note the lack of trigonal symmetry for the C vacancy.

indicate that C–C distances for the bonds pertaining to concave angles become shortened by 0.04 Å, in comparison with the regular graphene. The C–C distances for the more external C–C bonds, such as C2–C3, C6–C7 and C10–C11, undergo a negligible change. On the other hand, the distance between the vertices of concave angles undergo a significant modification: whereas C1–C5 and C1–C9 distances become stretched, *c.* 0.08 Å, the C5–C9 distance becomes shortened *c.* 0.16 Å. This observation is directly related to a modification of the concave angles: whereas one of them is much more closed; namely, the C12–C1–C2, *c.*6°, the other two are more

Table 3. E_{vac}, E_{relax} and geometrical parameters for the C vacancy.

		E_{vac} [eV]	E_{relax} [eV]	d_{C-C} [Å][a,b] C1–C2/C5–C6 (C9–C10)	d_{C-C} [Å][a,b] C1–C5 (C1-C9)/C5–C9	Concave C–C–C angle[O][a,c] C12–C1–C2/C4–C5–C6 (C8–C9–C10)
Cluster model	PBE	15.61	0.37	1.38/1.38 (−0.04)/(−0.04)	2.53/2.29 (0.07)/(−0.17)	234.8/241.4 (−5.5)/(1.7)
	B3LYP	15.39	0.41	1.38/1.38 (−0.04)/(−0.04)	2.55/2.30 (0.09)/(−0.15)	233.9/240.9 (−6.4)/(1.2)
Slab model	PBE	16.66	0.51	1.37/1.39 (−0.06)/(−0.04)	2.59/2.21 (0.12)/(−0.26)	232.9/242.2 (−7.1)/(2.4)
	B3LYP[d]	15.83	—	—	2.65/2.13	—

[a]The C atoms are labeled like in Fig. 2(b).
[b]Between brackets: change of C–C distance with respect to the value for bare perfect graphene.
[c]Between brackets: change of concave C–C–C angle with respect to the value for bare perfect graphene.
[d]Work of Ghigo *et al.*[35]

open, *c.* 1°–2°, in comparison with the regular surface. This means that the trigonal symmetry of regular graphene is broken. In other words, C1, C5 and C9 form a nonequilateral triangle with the C1–C5 and C1–C9 distances longer than the C5–C9 one. A similar behavior was reported by Ghigo *et al.*,[37] It is important to underline that this geometry is not an artifact produced by the cluster model approach because it is also observed when slabs are used (Table 3). Particularly, in our cluster model the carbon atoms of the border are not allowed to relax, imposing the geometry of the extended graphene layer. Otherwise, a more opened reconstructed geometrical structure is obtained, in comparison to that of slab models.[37]

The E_{vac} value obtained using PBE with the cluster model is nearly 1 eV smaller than that obtained with our slab model. In the latter approach, the E_{relax} term is also relatively minority; besides, from the geometrical data of Table 3 we observe that using the slab model the vacancy also shows a distorted geometry indicating that the trigonal symmetry has been broken. On the other hand, the E_{vac} value obtained with the cluster model but using the B3LYP functional is 0.35 eV smaller than one previously reported calculated with a Gaussian basis set and periodic conditions.[37]

In the calculations performed with the cluster model, both the singlet and triplet states of defective graphene were considered. The corresponding total energies indicate that the triplet state is more favored. The calculations performed with the slab model confirm that the magnetic state is more stable than the nonmagnetic, with a magnetic moment of 0.60 μ_B per cell. Regarding the spin distribution, it is mainly localized in the vacancy. To show this effect, in Fig. 3 the atomic SP values

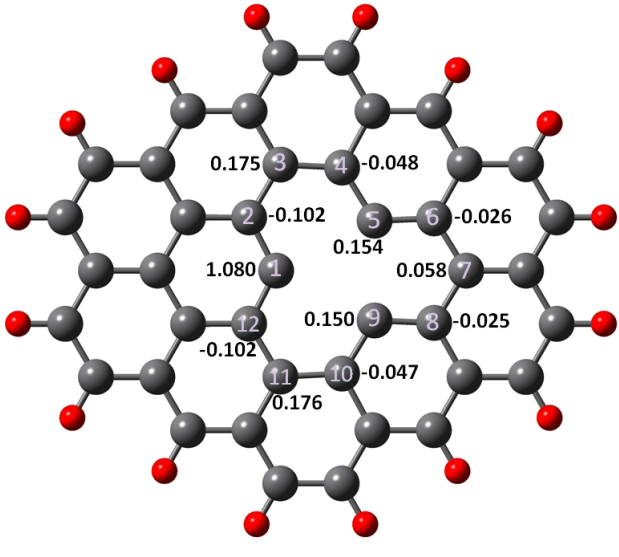

Fig. 3. (Color online) Atomic distribution of spin population for a graphene monovacancy (B3LYP functional, NPA Analysis). C atoms: large grey balls; H atoms: small red balls.

corresponding to the C atoms surrounding the vacancy are summarized. They were obtained from the α- and β-spin NPA populations calculated using the B3LYP functional and the cluster model. It is noteworthy that the spin localization on carbon atom C1 of the vacancy ring exhibits a relatively high atomic spin polarization in comparison with the corresponding value on carbon atoms C5 and C9. This is in good agreement with earlier calculations performed with periodic methods and plane waves[2,38,39] or Gaussian basis sets.[37] The former works reported a magnetic moment which ranges from $0.45\,\mu_B$ to $1.14\,\mu_B$ per defect. The low atomic spin polarization on C5 and C9 atoms is compatible to their dangling bonds coupling and the formation of a bond between them, with the resulting decrease of C5–C9 distance.[37] It was previously found that when a C monovacancy is created the high occupied molecular orbital is mainly localized on the defect site.[40]

The creation of a vacancy in graphene leaves three unsaturated carbon atoms, eventually increasing the adsorption capacity of this surface. In order to analyze this capacity in more detail, one of the most important local reactivity descriptors, the Fukui function $f(\vec{r})$, was used.[41] More specifically, the condensed definition of $f(\vec{r})$on the individual atom k of defective graphene for a radical attack[42] was calculated, f_k^0, taking into account that an individual Al atom can be considered a radical species from the reactivity point of view. In Fig. 4, the values of f_k^0 corresponding to the C atoms surrounding the vacancy are summarized. We observe that C1, C5 and C9 atoms have a condensed Fukui function value of about 0.06–0.07 that is much higher than for the other carbon atoms of the vacancy polygon. Contrastingly, a regular C atom of nondefective graphene has a condensed Fukui function value of 0.01.

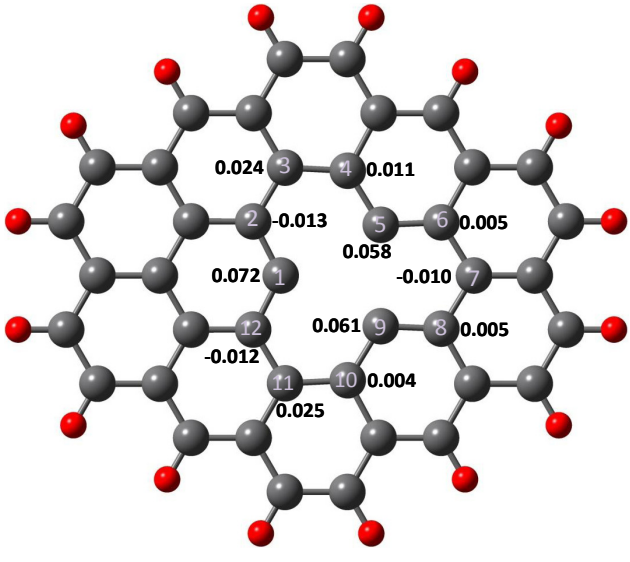

Fig. 4. (Color online) Atomic distribution of Fukui function for a graphene monovacancy (B3LYP functional, NPA analysis). C atoms: large grey balls; H atoms: small red balls.

Therefore, and despite of the absence of trigonal symmetry, it can be predicted from this local reactivity descriptor that these three carbon atoms are equally reactive for adsorption of Al atoms.

3.3. *Al adsorption on defective graphene*

After studying the creation of a monovacancy, we proceed to consider the adsorption of Al atom on this site. In Fig. 5, the optimized geometrical configuration in our cluster surface model corresponding to this adsorption site is schematized. The slab model was also schematized in the same figure. The E_{ads} values for both functionals and the main interatomic distances and deviations from planarity are summarized in Table 4.

Notice from Table 4 that both functionals give similar values for E_{ads} energies as well as for the Al–C distances. The adsorption energy values, *c.* −4.5 eV, indicate an important chemisorptive interaction in agreement with the calculated Al–C distances, *c.* 1.85 Å, that are 0.3 Å shorter than the sum of Al and C covalent radii and 0.1 Å–0.3Å shorter than the Al–C distance in trimethylaluminum. The Al

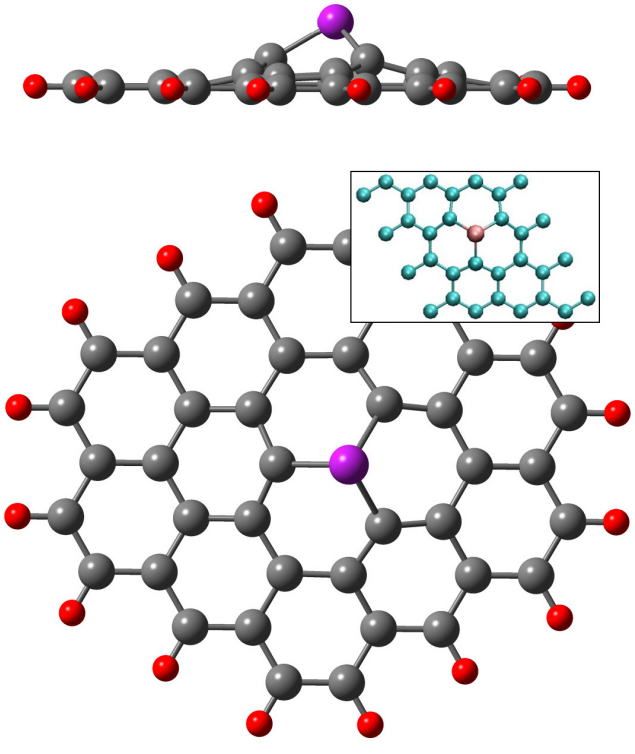

Fig. 5. (Color online) Cluster model for the adsorption geometry of Al adsorbed on a monovacancy of graphene. C atoms: large grey balls; Al atom: small purple ball; H atoms: small red balls. The inset shows the geometry with the slab model.
Top panel: Lateral view. Bottom panel: Top view.

Table 4. E_{ads}, E_{reac} and geometrical parameters for Al adsorption on defective graphene.

		E_{ads} [eV]	E_{reac} [eV]	d_{Al-C} [Å][a]	$d_{C-C'}$ [Å][b,c]	h_{Al} [Å]	h_C [Å][a]
Cluster model	PBE	−4.59	11.02	1.86	1.41 (−0.01)	1.64	0.68
	B3LYP	−4.46	10.93	1.84	1.41 (−0.02)	1.55	0.64
Slab model	PBE	−5.51	11.15	1.85	1.40 (−0.02)	1.38	0.53
	PBE[d]	—	10.06	1.86	—	—	—
	PBE[e]	—	—	1.85	—	—	—

[a]C: First nearest neighbor of Al atom (C1, C5 or C9, see Fig. 2(b)).
[b]C: First nearest neighbor of Al atom (C1, C5 or C9); C′: carbon first nearest neighbor of C1, C5 or C9 atom (see Fig. 2(b)).
[c]Values between brackets: change of $d_{C-C'}$ with respect to the value for bare perfect graphene.
[d]Work of Denis.[9]
[e]Works of Dai *et al.*,[13] and Dai and Yuan.[15]

atom is linked to the three C atoms that are vertexes of the concave angles described in the previous section and that exhibited the largest condensed Fukui function values. Apart from the configuration outlined in Fig. 5, another geometry was also obtained. In this case, the Al atom resides on the graphene plane with an Al–C distance of 1.68 Å giving an E_{ads} of −1.87 eV for the PBE functional. A similar geometry has previously been reported based on the PBE functional, a periodic approach and a local basis set.[13] By making an analysis of frequencies at this last geometry and that reported in Table 3 for PBE, we obtained that the former actually corresponds to a saddle point of potential energy surface (PES). A similar result with the B3LYP functional was obtained. This structure corresponds to a transition state between the adsorbed Al and another equivalent geometry on the other side of the graphene sheet.

An important conclusion from the above considerations is the fact that the adsorption of an Al atom on defective graphene is described similarly by PBE and B3LYP functionals unlike the case of adsorption on perfect graphene where these functionals show opposite behaviors. On perfect graphene, which has a closed shell electronic structure, an important repulsion probably due to exchange effects is computed with the B3LYP functional, whereas on defective graphene, which has a opened shell electronic structure, these effects are not present and both functional works more similarly.

The insertion of an Al atom in a graphene sheet can be described as the adsorption on a pre-existing monovacancy through the following reaction:

$$\text{Graphene} + \text{isolated Al atom} \rightarrow \text{Al/Graphene (on vacancy)} + \text{isolated C atom} \quad (4)$$

whose energy balance is defined as the reaction energy, E_{reac}. This energy can be calculated considering two contributions:

$$E_{reac} = E_{vac} + E_{ads}, \quad (5)$$

where E_{vac} and E_{ads} correspond to the monovacancy formation energy and the adsorption energy, respectively. Table 4 results indicate that both functionals give similar values for E_{reac} energies, *c.* 11 eV.

A large distortion is produced on the graphene geometry, as it can be appreciated by the side view of Fig. 5 and from the data of Table 4. Indeed, an important puckering of the graphene surface of about 0.6 Å–0.7 Å can be observed due to the upraising of the three C apical atoms linked to Al (C1, C5 and C9). The distances between these C atoms and their first C neighbors decrease only 0.01 Å–0.02 Å, in comparison with the bare regular graphene surface. On the other hand, the distances between the three apical atoms are very similar (2.77 Å) and the concave vacancy angles are almost the same (237°–238°), thus indicating that the trigonal symmetry has been recovered. The angle defined by the C1–Al bond and the plane containing C1–C12 and C1–C2 bonds present values that range between 183.0° and 184.5°; thus indicating a small distortion of about 3°–4.5° in comparison with C1 sp^2 hybridization.

The E_{ads} value obtained using PBE with the cluster model is nearly 1 eV less negative than that obtained with our slab model. In the latter approach, the Al–C distance is quite identical, though only 0.01 Å shorter, but the puckering of the graphene surface is 0.02 Å less upraised. The other geometrical changes suffered by the graphene surface present the same trend as those observed using the cluster model; in particular, the trigonal symmetry recovery. There are no reported E_{ads} values in the literature with which we can compare our results, nevertheless the E_{reac} value calculated in another work with the PBE functional, a periodic model approach and a Gaussian basis set[9] is *c.* 1 eV lower than our result; namely, 10.06 eV versus to 11.05 eV. On the other hand, the Al–C distance is very similar, 1.86 Å versus 1.85 Å. Besides, previous periodic calculations performed with PBE and plane waves, reported an Al–C distance identical to our result using a slab model.[13,15]

It is noteworthy that the E_{ads} magnitude for Al adsorption on a vacancy is noticeably greater than those obtained on regular graphene, indicating an important chemical interaction. In order to study the nature of this interaction, an NPA analysis of charge transfer was performed with the cluster approach and using the B3LYP functional. In Table 5, the main results are summarized. A relevant electronic transfer is produced between the Al atom and its three C neighbors, *c.* 0.8e, as

Table 5. NPA atomic net charge (Q), change of NPA atomic net charge (ΔQ) and atomic spin population (SP) for Al adsorption on defective graphene (Cluster model).

	Q[a] Al/C1/C5/C8	ΔQ[a,b] Al/C1/C5/C8	SP[a] Al/C1/C5/C8
PBE	1.43/ − 0.41/ − 0.48/ − 0.48	1.43/ − 0.61/ − 0.65/ − 0.60	0.18/0.23/ − 0.02/ − 0.02
B3LYP	1.56/ − 0.44/ − 0.51/ − 0.51	1.56/ − 0.66/ − 0.69/ − 0.63	0.19/0.20/ − 0.02/ − 0.02

[a]C: First nearest neighbor of Al atom, C1/C5/C8 (see Fig. 2(b)).
[b]Change of Q with respect to the value for bare defective graphene and neutral Al atom.

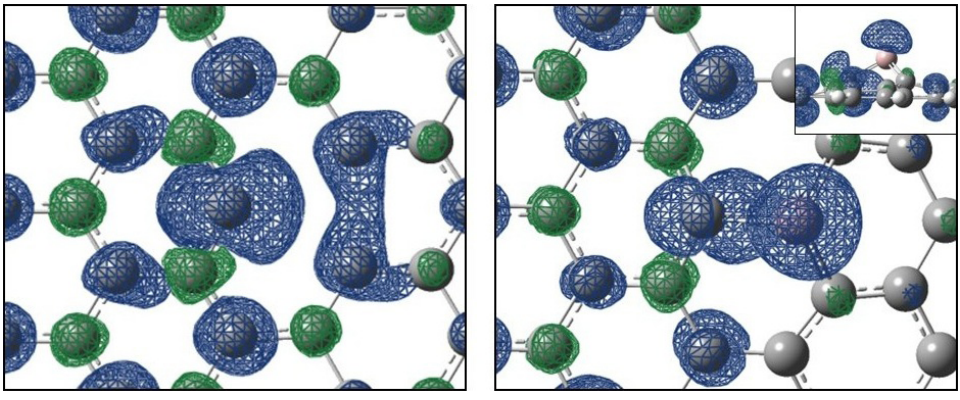

Fig. 6. (Color online) Spatial distribution of spin density for Al adsorbed on a monovacancy of graphene (B3LYP functional). Blue: spin-up electron density; green: spin-down electron density. Isovalue = 0.002 a.u. Left panel: bare monovacancy, top view. Right panel: Al on monovacancy, top view. Insert: lateral view.

can be appreciated by the net atomic NPA charges and the corresponding changes with respect to the bare defective surface.

In the calculations with the cluster model for the Al/defective-graphene system, the doublet state is more favored; thus indicating that for the vacancy, the unpaired electron of isolated Al atom couples with one unpaired electron of graphene, leaving the other one distributed over the surface. The calculations performed with the slab model confirm that the magnetic state is more stable than the nonmagnetic, with a magnetic moment of $0.3\,\mu_B$ per cell. Regarding the spin localization, calculations performed with the cluster model and using the B3LYP functional summarized in Table 5 show that *c.* 0.45 of the spin corresponding to the doublet configuration resides on the Al atom and their first neighboring C atoms. This picture can be compared with the value of 0.20–0.27 obtained for Al on the regular surface, clearly showing that the spin is more localized in the case of adsorption on the vacancy. The spatial distribution of the spin density around this carbon atom can be observed looking at Fig. 6(b) and compared to that of the bare monovacancy (Fig. 6(a)).

From the above quantitative and a qualitative analysis, we can also infer that differently from the results for Al adsorption on regular graphene, the insertion of an Al atom in graphene is described in a very similar way by both PBE and B3LYP functionals.

4. Conclusions

Calculations performed with the cluster approach reveal that depending on the theoretical treatment of electronic exchange and correlations effects, different bonding results are obtained for the adsorption of an Al atom on the regular surface of graphene.

The PBE functional shows that weak chemisorption is produced at Al-graphene distances of 2.1 Å–2.3 Å for the sites of high symmetry of a graphene sheet, with E_{ads} values of about −0.3 eV to −0.4 eV. Conversely, the results obtained with the B3LYP functional exhibit that the Al-graphene reaction is endothermic for hollow and bridge sites, with E_{ads}–0.1 eV, presenting somewhat larger Al-graphene distances, *c.* 0.05 Å–0.08 Å; moreover, no bonding is present on the on-top site. While an ionic interaction is present for both functionals, with an electron drift from the Al atom toward the carbon atoms, an important repulsion probably due to exchange effects is also observed with the B3LYP functional. The electron spin of Al becomes largely delocalized on the graphene surface. The results for the adsorption of Al on regular graphene obtained with the cluster model and using PBE have been contrasted with calculations performed with the slab model, reaching very near geometries and attaining E_{ads} values similar to those reported in previous periodic calculations. Neither of the two DFT functionals predicts the existence of physisorption states at large distances from the surface.

The formation of a carbon vacancy in a graphene sheet is very similarly described with both exchange and correlation functionals. This process demands about 15.5 eV and is accompanied with the loss of trigonal symmetry. Moreover, a spin polarization involving two electrons is produced, particularly localized on one of the vertexes of concave angles inside the vacancy. The three C atoms of these vertices become the more reactive to a radical attack, according to their condensed Fukui function values. The adsorption of an Al atom on this vacancy proceeds via the linking to these C atoms and yields a significant distortion on the graphene surface, upraising the C atoms, *c.* 0.5 Å–0.7 Å, but restoring the trigonal symmetry. These atoms show hybridization close to sp.[2] The adsorption energy and Al–C distances are very similar when both exchange and correlation functionals are used, *c.* − 4.5 eV and 1.86 Å, respectively. An electron drift is produced from the Al atom toward the carbon atoms; nevertheless, the spin polarization is highly localized on nearest C atoms due to an uncompensated spin.

Acknowledgments

The authors want to acknowledge the financial support of these Argentine institutions: Consejo Nacional de Investigaciones Científicas y Técnicas, Agencia Nacional de Promoción Científica y Tecnológica and Universidad Nacional del Sur.

References

1. Sevinçli H, Topsakal M, Durgun E, Ciraci S, Electronic and magnetic properties of 3d-transition metal atom adsorbed on graphene and graphene nanoribbons, *Phys Rev B* **77**:195434, 2008.
2. Singh R, Kroll P, Magnetism in graphene due to single-atom defects: dependence on the concentration and packing geometry of defects, *J Phys: Condens Matter* **21**:196002, 2009.

3. Chan KT, Neaton JB, Cohen ML, First-principle study of metal adatom adsorption on graphene, *Phys Rev B* **77**:235430, 2008.
4. Zhu ZH, Lu GQ, Comparative study of Li, Na and K adsorptions on graphite by using *ab initio* method, *Langmuir* **20**:10751–10755, 2004.
5. Ferre-Vilapalna A, Storage of hydrogen adsorbed on alkali metal doped single-layer all carbon materials, *J Phys Chem C* **112**:3998–4004, 2008.
6. Zhou L-J, Hou ZF, Wu LM, Fist-principles study of lithium adsorption and diffusion on graphene with point defects, *J Phys Chem C* **116**:21780–21787, 2012.
7. Ferro Y, Fernandez N, Allouche A, Linsmeier C, Adsorption of beryllium atoms and clusters both on graphene and in a bilayer of graphite investigated by DFT, *J Phys Condens Matter* **25**:015002, 2013.
8. Srivastava S, Almlöf J, Chemisorption of aluminum atoms on a graphite surface: Cluster convergence and effects of surface reconstruction, *Surf Sci* **274**:113–119, 1992.
9. Denis PA, Band gap opening of monolayer and bilayer graphene doped with aluminium, silicon, phosphorus, and sulfur, *Chem Phys Lett* **492**:251–257, 2010.
10. Schedin F, Geim AK, Morozov SV, Hill EW, Blake P, Katsnelson MI, Novoselov KS, Detection of individual gas molecules adsorbed on graphene, *Nat Mater* **6**:652–655, 2007.
11. Reddy D, Register LF, Carpenter GD, Banerjee SK, Graphene field-effect transistors, *J Phys D Appl Phys* **44**:313001, 2011.
12. Ao ZM, Yang J, Li S, Jiang Q, Enhancement of CO detection in Al doped graphene, *Chem Phys Lett* **461**:276–279, 2008.
13. Dai J, Yuan J, Giannozzi P, Gas adsorption on graphene doped with B, N, Al, and S: A theoretical study, *Appl Phys Lett* **95**:232105, 2009.
14. Zhang Y-H, Chen Y-B, Zhou KG, Liu CH, Zeng J, Zhang H-L, Peng Y, Improving gas sensing properties of graphene by introducing dopants and defects: A first-principles study, *Nanotechnology* **20**:185504, 2009.
15. Dai J, Yuan J, Adsorption of molecular oxygen on doped graphene: Atomic, electronic, and magnetic properties, *Phys Rev B* **81**:165414, 2010.
16. Chi M, Zhao Y-P, Adsorption of formaldehyde molecule on the intrinsic and Al-doped graphene: A first principle study, *Comp Mater Sci* **46**:1085–1090, 2009.
17. Frisch MJ, Trucks GW, Schlegal MB *et al.*, Gaussian 03, Revision D.01, Gaussian, Inc., Wallingford, CT, 2004.
18. Ferullo RM, Domancich NF, Castellani NJ, On the perfomance of van der Waals corrected-density functional theory in describing the atomic hydrogen physisorption on graphite, *Chem Phys Lett* **500**:283–286, 2010.
19. Ferro Y, Allouche A, Marinelli F, Brosset C, Theoretical study of oxygen adsorption on boron-doped graphite, *Surf Sci* **559**:158–168, 2004.
20. Rougeau N, Teillet-Billy D, Sidis V, Double H atom adsorption on a cluster model of a graphite surface, *Chem Phys Lett* **431**:135–138, 2006.
21. Bonfanti M, Martinazzo R, Tantardini G, Ponti A, Physisorption and diffusion of hydrogen atoms on graphite from correlated calculations on the H-coronene model system, *J Phys Chem C* **111**:5825–5829, 2007.
22. Su Y, Gao X, Zhao J, Reaction mechanisms of graphene oxide chemical reduction by sulfur-containing compounds, *Carbon* **67**:146–155, 2014.
23. Tachikawa H, Iyama T, Structures and electronic states of fluorinated graphene, *Solid State Sci* **28**:41–46, 2014.
24. Tachikawa H, Iyama T, Kawabata H, Effect of hydrogenation on the band gap of graphene nano-flakes, *Thin Solid Films* **554**:199–203, 2014.
25. Perdew JP, Burke K, Ernzerhof M, Generalized gradient approximation made simple, *Phys Rev Lett* **77**:3865–3868, 1996.

26. Becke AD, Density-functional thermochemistry. III. The role of exact exchange, *J Chem Phys* **98**:5648–5652, 1993.
27. Boys SF, Bernardi F, The calculation of small molecular interactions by the differences of separate total energies. Some procedures with reduced errors, *Mol Phys* **19**:553–566, 1970.
28. Reed AE, Curtiss LA, Weinhold F, Intermolecular interactions from a natural bond orbital, donor–acceptor viewpoint, *Chem Rev* **88**:899–926, 1988.
29. Kresse G, Furthmüller J, Efficient iterative schemes for *ab initio* total-energy calculations using a plane-wave basis set, *Phys Rev B* **54**:11169–11186, 1996.
30. Kresse G, Furthmüller J, Efficiency of *ab-initio* total energy calculations for metals and semiconductors using a plane-wave basis set, *Comput Mater Sci* **6**:15–50, 1996.
31. Blöchl P, Projector augmented-wave method, *Phys Rev B* **50**:17953–17979, 1994.
32. Kresse G, Joubert D, From ultrasoft pseudopotentials to the projector augmented-wave method, *Phys Rev B* **59**:1758–1775, 1999.
33. Monkhorst HJ, Pack JD, Special points for Brillouin-zone integrations, *Phys Rev B* **13**:5188–5192, 1976.
34. Holleman AF, Wiberg E, *Inorganic Chemistry*, Academic Press, San Diego, 2001.
35. Moullet I, *Ab-initio* molecular dynamics study of the interaction of aluminium clusters on a graphite surface, *Surf Sci* **331–333**:697–702, 1995.
36. Nakada K, Ishii A, Migration of adatom adsorption on graphene using DFT calculation, *Solid State Commun* **151**:13–16, 2011.
37. Ghigo G, Maranzana A, Tonachini G, Zicovich-Wilson CM, Causà M, Modeling soot and its functionalization under atmospheric or combustion conditions by density functional theory within molecular (polycyclic-aromatic-hydrocarbon-like) and periodic methodologies, *J Phys Chem B* **108**:3215–3223, 2004.
38. Lim D-H, Suarez Negreira A, Wilcox J, DFT studies on the interaction of defective graphene-supported Fe and Al nanoparticles, *J Phys Chem C* **115**:8961–8970, 2011.
39. Yazyev OV, Helm L, Defect-induced magnetism in graphene, *Phys Rev B* **75**:125408, 2007.
40. Tachikawa H, Nagoya Y, Kawabata H, A Density functional theory study of ground and low-lying excited electronic states in defective graphenes, *J Chem Theory Comput* **5**:2101–2107, 2009.
41. Parr RG, Yang W, Density functional approach to the frontier-electron theory of chemical reactivity, *J Am Chem Soc* **106**:4049–4050, 1984.
42. Yang W, Mortier WJ, The use of global and local molecular parameters for the analysis of the gas-phase basicity of amines, *J Am Chem Soc* **108**:5708–5711, 1986.